IEEE Open Journal of
Antennas and Propagation

Received 11 May 2020; revised 31 May 2020; accepted 30 June 2020. Date of publication 3 July 2020; date of current version 24 July 2020.

Digital Object Identifier 10.1109/OJAP.2020.3006842

Direct-Splitting-Based CN-FDTD for Modeling 2D Material Nanostructure Problems

NAIXING FENG [1] (Member, IEEE), YUXIAN ZHANG [1] (Member, IEEE), QINGSHENG ZENG [2] (Senior Member, IEEE), MEISONG TONG [3] (Senior Member, IEEE), WILLIAM T. JOINES [4] (Life Fellow, IEEE), AND GUO PING WANG [1]

[1] Institute of Microscale Optoelectronics, Shenzhen University, Shenzhen 518060, China

[2] College of Astronautics, Nanjing University of Aeronautics and Astronautics, Nanjing 210016, China

[3] Key Laboratory of Embedded System and Service Computing of the Ministry of Education, College of Electronics and Information Engineering, Tongji University, Shanghai 200092, China

[4] Department of Electrical and Computer Engineering, Duke University, Durham, NC 27708, USA

CORRESPONDING AUTHORS: Y. ZHANG AND G. P. WANG (e-mail: yxzhang_tute@126.com; gpwang@szu.edu.cn)

This work was supported in part by the National Nature Science Foundation of China under Grant 61901274; in part by the Shenzhen Science and Technology Innovation Committee under Grant JCYJ20190808141818890; and in part by the Guangdong Natural Science Foundation under Grant 2020A1515010467.

ABSTRACT Incorporating a truncation of the complex-frequency-shifted perfectly matched layer (CFS-PML), the direct-splitting- based Crank-Nicolson finite-difference time-domain (CNDS-FDTD) is developed and applied to the infrared two-dimensional layered material (2DLM) black phosphorous (BP) metasurface implementations on the all-dielectric nanostructure. To improve extremely low efficiencies in solving infrared terahertz (THz) problems with the few-atomic-layer thickness of 2DLMs, the CFS-CNDS-FDTD is proposed in demand due to the fact that it possesses capabilities of implicit FDTD method and unsplit-field CFS-PML truncation, respectively, in completely conquering the Courant-Friedrich-Levy condition (CFL) limit and holding good performance. The temporal incremental in the CFS-CNDS-FDTD can reach 1000 times larger than that in the regular FDTD for infrared nanoscale problems centered at the 2.5 THz and then keep accurate. Three-dimensional (3D) numerical cases have been carried out to corroborate the proposed method. The CFS-CNDS- FDTD can not only achieve high accuracies and then saves several dozen times of CPU time as compared to the regular FDTD, but also pave the way for designing all-dielectric nanostructures with other 2DLM metasurfaces.

INDEX TERMS Black phosphorous (BP), Crank-Nicolson finite-difference time-domain (CN-FDTD), complex-frequency-shifted perfectly matched layer (CFS-PML), direct-splitting (DS), metasurface, two-dimensional layered material (2DLM).

I. INTRODUCTION

THE METALLIC or dielectric metasurfaces [1]–[7] are composed of arrays of subwavelength-spaced optical scatters distributed atop the interface whose prime function is to allow for locally altering the phase of incident light, which have very recently drawn considerable attention due to the fact that a unique method can be provided to guide electromagnetic waves at will, and then possess advanced optical technology adopted for implementing versatile functionalities in a planar structure [8]–[14]. Therefore, the significant loss and fabrication difficulty of volumetric metamaterials can be effectively avoided [2], [15]–[16].

However, as far as we know, most previously elaborated metasurface designs encounter low coupling efficiency and are based on metallic resonators, which leads to ohmic loss.

To overcome drawbacks of plasmonic metasurfaces, one can replace metals with all-dielectric resonators [17], [18]. Dielectric metasurfaces consist of interfaces patterned with a distribution of high-index dielectric light scattering particles of size comparable to the wavelength of light [3]. Their scattering properties were first studied by Faraday [19] and the effect is also known as Faraday-Tyndall scattering.

Very recently, an efficient design of all-dielectric photonic structure has been implemented for modeling graphene-based

optoelectronics devices, which provide a promising method applied to enhancing light-matter interaction in sub-nanometer two-dimensional layered materials (2DLMs) [20]. Furthermore, black phosphorous (BP), as another emerging member of the 2DLMs, has exhibited high carrier mobility, strong light-matter interaction in the infrared spectrum, and high degree of band anisotropy [21]–[25]. Besides, fully different from graphene with in-plane isotropy, the BP shows in-plane anisotropic properties. Therefore, the monolayer 2D BP with/without subwavelength patterning will be added into 3D all-dielectric nanostructures in this study.

However, the monolayer BP is few-atomic-layer thickness in size, and hence relatively thin as compared with the regular 3D geometrical nanostructures, leading to requirements of massive CPU time and computer memory for regular finite-difference time-domain (FDTD) simulations [26]–[34] because of resulting from the Courant-Friedrich-Levy condition (CFL) limit. The challenge lies in a quite large number of time steps required by the regular FDTD method for infrared sub-nanometer problems where high spatial and temporal sampling densities are required. For example, at the central frequency of 1 terahertz (THz) in the all-dielectric nanostructure application, spatial and temporal sampling densities in air can be approximately 0.1 million points per wavelength (PPW) and 0.3 million points per period (PPP), separately. To circumvent this problem, implicit FDTD methods [35]–[38] can be well used, which encounter no limit on time intervals arising from stability considerations.

The Crank-Nicolson FDTD (CN-FDTD) methods, as one of the most popular implicit formulations, are characterized with pretty high numerical accuracies and exhibit extremely small numerical anisotropy, but their full implicit discretization leads to a huge sparse matrix that needs to be inverted [39].

Very recently, to avoid solving very huge sparse matrix so that the CPU time and memory can be dramatically decreased, the cycle-sweep-uniform CN-FDTD (CNCSU-FDTD) is used to solve 3D low frequency subsurface sensing problems [40], which can be also used for modeling 3D infrared all-dielectric nanostructures with a 2D BP with the design of metasurface. However, it should be noted that the ADE-based CFS-CNCSU -FDTD method is indicated in [40], [41] to be only conditionally stable in certain situations. Recently, however, the BT-based CNDS-FDTD method is proposed and applied to solve FDTD problems in the microwave range, and then further prove that the CNCSU-FDTD exists the instability in certain cases [42].

In this systematic study, the efficient direct-splitting-based CN-FDTD (CNDS-FDTD) method with the CFS-PML scheme is proposed based on the auxiliary differential equation (ADE) method to model 3D all-dielectric photonic nanostructures with monolayer BP metasurfaces in the infrared Terahertz range. The CFS-CNDS-FDTD not only possess higher efficiency than the alternating-direction-implicit FDTD (ADI-FDTD) method [43]–[46] due to owning fewer loops at each time step, but is suitable for parallel computation [47]–[49] which can be used to further reduce CPU time [39].

In view of the CFL limit of regular FDTD method needing higher PPW and PPP sampling, the CFS-CNDS-FDTD method is adopted to overcome extremely low computational efficiency by using large CFL number (CFLN). For example, the CFLN = 1000 can be set, and hence several dozen times of CPU time as compared with the regular FDTD method can be saved. Besides, to further corroborate the performance of CFS-CNDS-FDTD, we design the 3D all-dielectric nanostructures adding the single layer BP with/without subwavelength patterning for validation. As a result, 3D numerical simulations have been carried out to prove that the proposed CFS-CNDS-FDTD not only saves a large amount of CPU time and then reaches good accuracies as compared with the conventional FDTD simulation, but paves the way for fabricating the all-dielectric nanostructures with BP and other 2DLM metasurfaces.

The main contributions of this work include following: (1) The unconditionally-stable CNDS-based FDTD formulations is developed, different from the CNCSU-based FDTD which is conditionally stable in certain cases; (2) The 3D all-dielectric nanostructures with BP metasurfaces in the infrared range are implemented using the CFS-CNDS-FDTD.

II. FORMULATION

In a 3D CFS-PML region, the frequency domain modified Maxwell's curl equations can be written as

$$j\omega\varepsilon_0\varepsilon_r(\omega)E(\omega)+\sigma E(\omega)=\nabla_s\times H(\omega) \tag{1}$$

$$j\omega\mu_0 H(\omega)=-\nabla_s\times E(\omega) \tag{2}$$

where $\varepsilon_r(\omega)$ and $\mu_r(\omega)$ are the relative permittivity and permeability of an inhomogeneous medium, respectively, and σ is the electrical conductivity. For the CFS-PML region, the operator ∇_s is expressed as

$$\nabla_s=\sum_{\eta=x,y,z}\hat{\eta}\,S_\eta^{-1}\partial_\eta \tag{3}$$

where ∂_x, ∂_y and ∂_z are partial derivatives with respect to x, y and z, and S_η is complex stretching coordinate metric with the CFS scheme, defined as

$$S_\eta=\kappa_\eta+\sigma_\eta/\left(\alpha_\eta+j\omega\right),\ (\eta=x,y,z) \tag{4}$$

where κ_η is a scaling factor, and imaginary part σ_η represents a loss in PML regions, and α_η is assumed to be positive real.

As an example, we now are considering discretization of the x component of E field in all corners and edges of PML regions that is parallel to the x direction

$$j\omega\varepsilon_0\varepsilon_r E_x+\sigma E_x=S_y^{-1}\frac{\partial H_z}{\partial y}-S_z^{-1}\frac{\partial H_y}{\partial z} \tag{5}$$

$$-j\omega\mu_0 H_y=S_z^{-1}\frac{\partial E_x}{\partial z}-S_x^{-1}\frac{\partial E_z}{\partial x} \tag{6}$$

$$-j\omega\mu_0 H_z=S_x^{-1}\frac{\partial E_y}{\partial x}-S_y^{-1}\frac{\partial E_x}{\partial y} \tag{7}$$

Rewrite S_η^{-1}, $(\eta = x, y, z)$ as

$$S_\eta^{-1} = (\kappa_\eta)^{-1} - \frac{\sigma_\eta / (\kappa_\eta^2 \varepsilon_0)}{j\omega + (\alpha_\eta + \sigma_\eta/\kappa_\eta)/\varepsilon_0} \tag{8}$$

Incorporating (8) into (5-7), and we have

$$\begin{aligned} j\omega\varepsilon_0\varepsilon_r E_x + \sigma E_x = {} & (\kappa_y)^{-1}\frac{\partial H_z}{\partial y} - (\kappa_z)^{-1}\frac{\partial H_y}{\partial z} \\ & - \frac{\sigma_y/(\kappa_y^2\varepsilon_0)}{j\omega + (\alpha_y + \sigma_y/\kappa_y)/\varepsilon_0}\frac{\partial H_z}{\partial y} \\ & + \frac{\sigma_z/(\kappa_z^2\varepsilon_0)}{j\omega + (\alpha_z + \sigma_z/\kappa_z)/\varepsilon_0}\frac{\partial H_y}{\partial z} \end{aligned} \tag{9}$$

$$\begin{aligned} j\omega\mu_0 H_y = {} & (\kappa_x)^{-1}\frac{\partial E_z}{\partial x} - (\kappa_z)^{-1}\frac{\partial E_x}{\partial z} \\ & - \frac{\sigma_x/(\kappa_x^2\varepsilon_0)}{j\omega + (\alpha_x + \sigma_x/\kappa_x)/\varepsilon_0}\frac{\partial E_z}{\partial x} \\ & + \frac{\sigma_z/(\kappa_z^2\varepsilon_0)}{j\omega + (\alpha_z + \sigma_z/\kappa_z)/\varepsilon_0}\frac{\partial E_x}{\partial z} \end{aligned} \tag{10}$$

$$\begin{aligned} j\omega\mu_0 H_z = {} & (\kappa_y)^{-1}\frac{\partial E_x}{\partial y} - (\kappa_x)^{-1}\frac{\partial E_y}{\partial x} \\ & - \frac{\sigma_y/(\kappa_y^2\varepsilon_0)}{j\omega + (\alpha_y + \sigma_y/\kappa_y)/\varepsilon_0}\frac{\partial E_x}{\partial y} \\ & + \frac{\sigma_x/(\kappa_x^2\varepsilon_0)}{j\omega + (\alpha_x + \sigma_x/\kappa_x)/\varepsilon_0}\frac{\partial E_y}{\partial x} \end{aligned} \tag{11}$$

To simplify (9-11), $f_{xy}, f_{xz}, g_{yx}, g_{yz}, g_{zx}, g_{zy}$are introduced as auxiliary variables, shown below

$$f_{xy} = \frac{\sigma_y/(\kappa_y^2\varepsilon_0)}{j\omega + (\alpha_y + \sigma_y/\kappa_y)/\varepsilon_0}\frac{\partial H_z}{\partial y} \tag{12}$$

$$f_{xz} = \frac{\sigma_z/(\kappa_z^2\varepsilon_0)}{j\omega + (\alpha_z + \sigma_z/\kappa_z)/\varepsilon_0}\frac{\partial H_y}{\partial z} \tag{13}$$

$$g_{yx} = \frac{\sigma_x/(\kappa_x^2\varepsilon_0)}{j\omega + (\alpha_x + \sigma_x/\kappa_x)/\varepsilon_0}\frac{\partial E_z}{\partial x} \tag{14}$$

$$g_{yz} = \frac{\sigma_z/(\kappa_z^2\varepsilon_0)}{j\omega + (\alpha_z + \sigma_z/\kappa_z)/\varepsilon_0}\frac{\partial E_x}{\partial z} \tag{15}$$

$$g_{zy} = \frac{\sigma_y/(\kappa_y^2\varepsilon_0)}{j\omega + (\alpha_y + \sigma_y/\kappa_y)/\varepsilon_0}\frac{\partial E_x}{\partial y} \tag{16}$$

$$g_{zx} = \frac{\sigma_x/(\kappa_x^2\varepsilon_0)}{j\omega + (\alpha_x + \sigma_x/\kappa_x)/\varepsilon_0}\frac{\partial E_y}{\partial x} \tag{17}$$

Substituting (12-17) into (9-11), and then adopting the auxiliary differential equation (ADE) technique, we obtain

$$\begin{aligned} \varepsilon_0\varepsilon_r\frac{\partial E_x}{\partial t} + \sigma E_x = {} & (\kappa_y)^{-1}\frac{\partial H_z}{\partial y} \\ & - (\kappa_z)^{-1}\frac{\partial H_y}{\partial z} - f_{xy} + f_{xz} \end{aligned} \tag{18}$$

$$\begin{aligned} \mu_0\frac{\partial H_y}{\partial t} = {} & (\kappa_x)^{-1}\frac{\partial E_z}{\partial x} - (\kappa_z)^{-1}\frac{\partial E_x}{\partial z} \\ & - g_{yx} + g_{yz} \end{aligned} \tag{19}$$

$$\begin{aligned} \mu_0\frac{\partial H_z}{\partial t} = {} & (\kappa_y)^{-1}\frac{\partial E_x}{\partial y} - (\kappa_x)^{-1}\frac{\partial E_y}{\partial x} \\ & - g_{zy} + g_{zx} \end{aligned} \tag{20}$$

$$\frac{\partial f_{xy}}{\partial t} + \frac{\alpha_y + \sigma_y/\kappa_y}{\varepsilon_0}f_{xy} = \frac{\sigma_y}{\kappa_y^2\varepsilon_0}\frac{\partial H_z}{\partial y} \tag{21}$$

$$\frac{\partial f_{xz}}{\partial t} + \frac{\alpha_z + \sigma_z/\kappa_z}{\varepsilon_0}f_{xz} = \frac{\sigma_z}{\kappa_z^2\varepsilon_0}\frac{\partial H_y}{\partial z} \tag{22}$$

$$\frac{\partial g_{yx}}{\partial t} + \frac{\alpha_x + \sigma_x/\kappa_x}{\varepsilon_0}g_{yx} = \frac{\sigma_x}{\kappa_x^2\varepsilon_0}\frac{\partial E_z}{\partial x} \tag{23}$$

$$\frac{\partial g_{yz}}{\partial t} + \frac{\alpha_z + \sigma_z/\kappa_z}{\varepsilon_0}g_{yz} = \frac{\sigma_z}{\kappa_z^2\varepsilon_0}\frac{\partial E_x}{\partial z} \tag{24}$$

$$\frac{\partial g_{zy}}{\partial t} + \frac{\alpha_y + \sigma_y/\kappa_y}{g_{zy}}g_{zy} = \frac{\sigma_y}{\kappa_y^2\varepsilon_0}\frac{\partial E_x}{\partial y} \tag{25}$$

$$\frac{\partial g_{zx}}{\partial t} + \frac{\alpha_x + \sigma_x/\kappa_x}{\varepsilon_0}g_{zx} = \frac{\sigma_x}{\kappa_x^2\varepsilon_0}\frac{\partial E_y}{\partial x} \tag{26}$$

Subsequently, applying the Crank-Nicolson method to (18)-(26), and then tidy them up, as in (27), shown at the bottom of the page, and (28)–(35), shown at the bottom of the next page.

$$\begin{aligned} & E_x^{n+1}\left(i+\frac{1}{2},j,k\right) \\ & = C_{exe}E_x^n\left(i+\frac{1}{2},j,k\right) \\ & \quad + C_{exhz}(j)\frac{1}{\Delta y}\left[H_z^{n+1}\left(i+\frac{1}{2},j+\frac{1}{2},k\right) - H_z^{n+1}\left(i+\frac{1}{2},j-\frac{1}{2},k\right) + H_z^n\left(i+\frac{1}{2},j+\frac{1}{2},k\right) - H_z^n\left(i+\frac{1}{2},j-\frac{1}{2},k\right)\right] \\ & \quad - C_{exhy}(k)\frac{1}{\Delta z}\left[H_y^{n+1}\left(i+\frac{1}{2},j,k+\frac{1}{2}\right) - H_y^{n+1}\left(i+\frac{1}{2},j,k-\frac{1}{2}\right) + H_y^n\left(i+\frac{1}{2},j,k+\frac{1}{2}\right) - H_y^n\left(i+\frac{1}{2},j,k-\frac{1}{2}\right)\right] \\ & \quad - C_{exf}\left[f_{xy}^{n+1}\left(i+\frac{1}{2},j,k\right) + f_{xy}^n\left(i+\frac{1}{2},j,k\right)\right] + C_{exf}\left[f_{xz}^{n+1}\left(i+\frac{1}{2},j,k\right) + f_{xz}^n\left(i+\frac{1}{2},j,k\right)\right] \end{aligned} \tag{27}$$

Next, substituting (30)–(35) into (27)–(29), we have (36)–(38), as shown at the bottom of the next page, where $D_\eta, (\eta = x, y, \text{ and } z)$ are central difference derivative approximations [13], and then temporary variables are shown below

$$C_{exe} = \frac{1 - \frac{\sigma \Delta t}{2\varepsilon_0 \varepsilon_r}}{1 + \frac{\sigma \Delta t}{2\varepsilon_0 \varepsilon_r}},$$

$$C_{exhz}(j) = \frac{\frac{\Delta t}{2\varepsilon_0 \varepsilon_r}}{1 + \frac{\sigma \Delta t}{2\varepsilon_0 \varepsilon_r}} \left[\kappa_{pml\_y}(j)\right]^{-1},$$

$$C_{exhy}(k) = \frac{\frac{\Delta t}{2\varepsilon_0 \varepsilon_r}}{1 + \frac{\sigma \Delta t}{2\varepsilon_0 \varepsilon_r}} \left[\kappa_{pml\_z}(k)\right]^{-1},$$

$$C_{exf} = \frac{\frac{\Delta t}{2\varepsilon_0 \varepsilon_r}}{1 + \frac{\sigma \Delta t}{2\varepsilon_0 \varepsilon_r}},$$

$$C_{hyez}\left(i + \frac{1}{2}\right) = \frac{\Delta t}{2\mu_0 \mu_r} \left[\kappa^*_{pml\_x}\left(i + \frac{1}{2}\right)\right]^{-1},$$

$$C_{hyex}\left(k + \frac{1}{2}\right) = \frac{\Delta t}{2\mu_0 \mu_r} \left[\kappa^*_{pml\_z}\left(k + \frac{1}{2}\right)\right]^{-1},$$

$$\begin{aligned}
H_y^{n+1}\left(i+\frac{1}{2},j,k+\frac{1}{2}\right) &= H_y^n\left(i+\frac{1}{2},j,k+\frac{1}{2}\right) \\
&+ C_{hyez}\left(i+\frac{1}{2}\right)\frac{1}{\Delta x}\left[E_z^{n+1}\left(i+1,j,k+\frac{1}{2}\right) - E_z^{n+1}\left(i,j,k+\frac{1}{2}\right) + E_z^n\left(i+1,j,k+\frac{1}{2}\right) - E_z^n\left(i,j,k+\frac{1}{2}\right)\right] \\
&- C_{hyex}\left(k+\frac{1}{2}\right)\frac{1}{\Delta z}\left[E_x^{n+1}\left(i+\frac{1}{2},j,k+1\right) - E_x^{n+1}\left(i+\frac{1}{2},j,k\right) + E_x^n\left(i+\frac{1}{2},j,k+1\right) - E_x^n\left(i+\frac{1}{2},j,k\right)\right] \\
&- C_{hyg}\left[g_{yx}^{n+1}\left(i+\frac{1}{2},j,k+\frac{1}{2}\right) + g_{yx}^n\left(i+\frac{1}{2},j,k+\frac{1}{2}\right)\right] + C_{hyg}\left[g_{yz}^{n+1}\left(i+\frac{1}{2},j,k+\frac{1}{2}\right) + g_{yz}^n\left(i+\frac{1}{2},j,k+\frac{1}{2}\right)\right] \qquad (28)
\end{aligned}$$

$$\begin{aligned}
H_z^{n+1}\left(i+\frac{1}{2},j+\frac{1}{2},k\right) &= H_z^n\left(i+\frac{1}{2},j+\frac{1}{2},k\right) \\
&+ C_{hzex}\left(j+\frac{1}{2}\right)\frac{1}{\Delta y}\left[E_x^{n+1}\left(i+\frac{1}{2},j+1,k\right) - E_x^{n+1}\left(i+\frac{1}{2},j,k\right) + E_x^n\left(i+\frac{1}{2},j+1,k\right) - E_x^n\left(i+\frac{1}{2},j,k\right)\right] \\
&- C_{hzey}\left(i+\frac{1}{2}\right)\frac{1}{\Delta x}\left[E_y^{n+1}\left(i+1,j+\frac{1}{2},k\right) - E_y^{n+1}\left(i,j+\frac{1}{2},k\right) + E_y^n\left(i+1,j+\frac{1}{2},k\right) - E_y^n\left(i,j+\frac{1}{2},k\right)\right] \\
&- C_{hzg}\left[g_{zy}^{n+1}\left(i+\frac{1}{2},j+\frac{1}{2},k\right) + g_{zy}^{n+1}\left(i+\frac{1}{2},j+\frac{1}{2},k\right)\right] + C_{hzg}\left[g_{zx}^{n+1}\left(i+\frac{1}{2},j+\frac{1}{2},k\right) + g_{zx}^{n+1}\left(i+\frac{1}{2},j+\frac{1}{2},k\right)\right] \qquad (29)
\end{aligned}$$

$$\begin{aligned}
f_{xy}^{n+1}\left(i+\frac{1}{2},j,k\right) &= C_{fxyf}(j) f_{xy}^n\left(i+\frac{1}{2},j,k\right) \\
&+ C_{fxyhz}(j)\frac{1}{\Delta y}\left[H_z^{n+1}\left(i+\frac{1}{2},j+\frac{1}{2},k\right) - H_z^{n+1}\left(i+\frac{1}{2},j-\frac{1}{2},k\right) + H_z^n\left(i+\frac{1}{2},j+\frac{1}{2},k\right) - H_z^n\left(i+\frac{1}{2},j-\frac{1}{2},k\right)\right] \qquad (30)
\end{aligned}$$

$$\begin{aligned}
f_{xz}^{n+1}\left(i+\frac{1}{2},j,k\right) &= C_{fxzf}(k) f_{xz}^n\left(i+\frac{1}{2},j,k\right) \\
&+ C_{fxzhy}(k)\frac{1}{\Delta z}\left[H_y^{n+1}\left(i+\frac{1}{2},j,k+\frac{1}{2}\right) - H_y^{n+1}\left(i+\frac{1}{2},j,k-\frac{1}{2}\right) + H_y^n\left(i+\frac{1}{2},j,k+\frac{1}{2}\right) - H_y^n\left(i+\frac{1}{2},j,k-\frac{1}{2}\right)\right] \qquad (31)
\end{aligned}$$

$$\begin{aligned}
g_{yx}^{n+1}\left(i+\frac{1}{2},j,k+\frac{1}{2}\right) &= C_{gyxg}\left(i+\frac{1}{2}\right) g_{yx}^n\left(i+\frac{1}{2},j,k+\frac{1}{2}\right) \\
&+ C_{gyxez}\left(i+\frac{1}{2}\right)\frac{1}{\Delta x}\left[E_z^{n+1}\left(i+1,j,k+\frac{1}{2}\right) - E_z^{n+1}\left(i,j,k+\frac{1}{2}\right) + E_z^n\left(i+1,j,k+\frac{1}{2}\right) - E_z^n\left(i,j,k+\frac{1}{2}\right)\right] \qquad (32)
\end{aligned}$$

$$\begin{aligned}
g_{yz}^{n+1}\left(i+\frac{1}{2},j,k+\frac{1}{2}\right) &= C_{gyzg}\left(k+\frac{1}{2}\right) g_{yz}^n\left(i+\frac{1}{2},j,k+\frac{1}{2}\right) \\
&+ C_{gyzex}\left(k+\frac{1}{2}\right)\frac{1}{\Delta z}\left[E_x^{n+1}\left(i+\frac{1}{2},j,k+1\right) - E_x^{n+1}\left(i+\frac{1}{2},j,k\right) + E_x^n\left(i+\frac{1}{2},j,k+1\right) - E_x^n\left(i+\frac{1}{2},j,k\right)\right] \qquad (33)
\end{aligned}$$

$$\begin{aligned}
g_{zy}^{n+1}\left(i+\frac{1}{2},j+\frac{1}{2},k\right) &= C_{gzyg}\left(j+\frac{1}{2}\right) g_{zy}^n\left(i+\frac{1}{2},j+\frac{1}{2},k\right) \\
&+ C_{gzyex}\left(j+\frac{1}{2}\right)\frac{1}{\Delta y}\left[E_x^{n+1}\left(i+\frac{1}{2},j+1,k\right) - E_x^{n+1}\left(i+\frac{1}{2},j,k\right) + E_x^n\left(i+\frac{1}{2},j+1,k\right) - E_x^n\left(i+\frac{1}{2},j,k\right)\right] \qquad (34)
\end{aligned}$$

$$\begin{aligned}
g_{zx}^{n+1}\left(i+\frac{1}{2},j+\frac{1}{2},k\right) &= C_{gzxg}\left(i+\frac{1}{2}\right) g_{zx}^n\left(i+\frac{1}{2},j+\frac{1}{2},k\right) \\
&+ C_{gzxey}\left(i+\frac{1}{2}\right)\frac{1}{\Delta x}\left[E_y^{n+1}\left(i+1,j+\frac{1}{2},k\right) - E_y^{n+1}\left(i,j+\frac{1}{2},k\right) + E_y^n\left(i+1,j+\frac{1}{2},k\right) - E_y^n\left(i,j+\frac{1}{2},k\right)\right] \qquad (35)
\end{aligned}$$

$$C_{hyg} = \frac{\Delta t}{2\mu_0\mu_r},$$
$$C_{hzex}\left(j+\frac{1}{2}\right) = \frac{\Delta t}{2\mu_0\mu_r}\left[\kappa^*_{pml\_y}\left(j+\frac{1}{2}\right)\right]^{-1},$$
$$C_{hzey}\left(i+\frac{1}{2}\right) = \frac{\Delta t}{2\mu_0\mu_r}\left[\kappa^*_{pml\_x}\left(i+\frac{1}{2}\right)\right]^{-1},$$
$$C_{hzg} = \frac{\Delta t}{2\mu_0\mu_r},$$

Similarly, same operations can be applied to other field components. Therefore, these all equations can be written compactly as

$$(I - D_1 - D_2)W^{n+1} = (U + D_1 + D_2)W^n + V \quad (39)$$

Eq. (39) can be factorized and split as

$$(I - D_1)W^* = (U + D_1 + 2D_2)W^n + V \quad (40)$$
$$(I - D_2)W^{n+1} = W^* - D_2W^n \quad (41)$$

It can be seen that (40)-(41) solve tri-diagonal matrices at each time step to obtain electric field components, while all magnetic field components can be found explicitly.

III. NUMERICAL RESULTS

As mentioned above, we have demonstrated and derived the CFS-CNDS-FDTD formulations, which can be efficiently and accurately utilized to model BP metasurface implementations in the infrared range. To further elaborate and corroborate advantages and applications of the CFS-CNDS-FDTD versus the regular FDTD in solving all-dielectric nanostructures, 3D numerical simulations are carried out to compare the accuracy and the efficiency and accuracy between both the CFS-CNDS- FDTD and the conventional FDTD.

As known to all, the numerical stability of the conventional FDTD method is determined by the CFL condition, which requires that the temporal incremental Δt has a specific bound relative to the lattice 3D-space size $\{\Delta x, \Delta y, \Delta z\}$. Therefore, the CFL factor can be defined in the w-direction as

$$s_w = \frac{c_0\Delta t}{\sqrt{3}\Delta w} \quad (w = x, y, z) \quad (42)$$

where Δw is the grid scale for FDTD. c_0 is the light speed in vacuum. The CFL factor must satisfy $s_w \leq 1$ in the

$$\begin{aligned}
&E_x^{n+1}\left(i+\frac{1}{2},j,k\right) + \left[C_{exhy}(k) - C_{exf}C_{fxzhy}(k)\right]D_zH_y^{n+1}\left(i+\frac{1}{2},j,k+\frac{1}{2}\right) - \left[C_{exhz}(j) - C_{exf}C_{fxyhz}(j)\right]D_yH_z^{n+1}\left(i+\frac{1}{2},j+\frac{1}{2},k\right)\\
&= C_{exe}E_x^n\left(i+\frac{1}{2},j,k\right) - \left[C_{exhy}(k) - C_{exf}C_{fxzhy}(k)\right]D_zH_y^n\left(i+\frac{1}{2},j,k+\frac{1}{2}\right)\\
&\quad + \left[C_{exhz}(j) - C_{exf}C_{fxyhz}(j)\right]D_yH_z^n\left(i+\frac{1}{2},j+\frac{1}{2},k\right)\\
&\quad - C_{exf}\left[\left[1 + C_{fxyf}(j)\right]f_{xy}^n\left(i+\frac{1}{2},j,k\right)\right] + C_{exf}\left[1 + C_{fxzf}(k)\right]f_{xz}^n\left(i+\frac{1}{2},j,k\right)
\end{aligned} \quad (36)$$

$$\begin{aligned}
&H_y^{n+1}\left(i+\frac{1}{2},j,k+\frac{1}{2}\right) + \left[C_{hyex}\left(k+\frac{1}{2}\right) - C_{hyg}C_{gyzex}\left(k+\frac{1}{2}\right)\right]D_zE_x^{n+1}\left(i+\frac{1}{2},j,k\right)\\
&\quad - \left[C_{hyez}\left(i+\frac{1}{2}\right) - C_{hyg}C_{gyxez}\left(i+\frac{1}{2}\right)\right]D_xE_z^{n+1}\left(i,j,k+\frac{1}{2}\right)\\
&= H_y^n\left(i+\frac{1}{2},j,k+\frac{1}{2}\right) - \left[C_{hyex}\left(k+\frac{1}{2}\right) - C_{hyg}C_{gyzex}\left(k+\frac{1}{2}\right)\right]D_zE_x^n\left(i+\frac{1}{2},j,k\right)\\
&\quad + \left[C_{hyez}\left(i+\frac{1}{2}\right) - C_{hyg}C_{gyxez}\left(i+\frac{1}{2}\right)\right]D_xE_z^n\left(i,j,k+\frac{1}{2}\right)\\
&\quad - C_{hyg}\left[1 + C_{gyxg}\left(i+\frac{1}{2}\right)\right]g_{yx}^n\left(i+\frac{1}{2},j,k+\frac{1}{2}\right) + C_{hyg}\left[1 + C_{gyzg}\left(k+\frac{1}{2}\right)\right]g_{yz}^n\left(i+\frac{1}{2},j,k+\frac{1}{2}\right)
\end{aligned} \quad (37)$$

$$\begin{aligned}
&H_z^{n+1}\left(i+\frac{1}{2},j+\frac{1}{2},k\right) - \left[C_{hzex}\left(j+\frac{1}{2}\right) - C_{hzg}C_{gzyex}\left(j+\frac{1}{2}\right)\right]D_yE_x^{n+1}\left(i+\frac{1}{2},j,k\right)\\
&\quad + \left[C_{hzey}\left(i+\frac{1}{2}\right) - C_{hzg}C_{gzxey}\left(i+\frac{1}{2}\right)\right]D_xE_y^{n+1}\left(i,j+\frac{1}{2},k\right)\\
&= H_z^n\left(i+\frac{1}{2},j+\frac{1}{2},k\right) + \left[C_{hzex}\left(j+\frac{1}{2}\right) - C_{hzg}C_{gzyex}\left(j+\frac{1}{2}\right)\right]D_yE_x^n\left(i+\frac{1}{2},j,k\right)\\
&\quad - \left[C_{hzey}\left(i+\frac{1}{2}\right) - C_{hzg}C_{gzxey}\left(i+\frac{1}{2}\right)\right]D_xE_y^n\left(i,j+\frac{1}{2},k\right)\\
&\quad - C_{hzg}\left[1 + C_{gzyg}\left(j+\frac{1}{2}\right)\right]g_{zy}^n\left(i+\frac{1}{2},j+\frac{1}{2},k\right) + C_{hzg}\left[1 + C_{gzxg}\left(i+\frac{1}{2}\right)\right]g_{zx}^n\left(i+\frac{1}{2},j+\frac{1}{2},k\right)
\end{aligned} \quad (38)$$

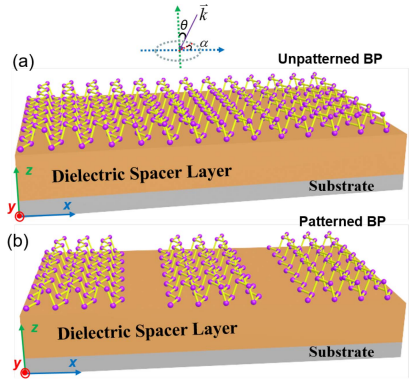

FIGURE 1. (a) Proposed nanostructure with unpatterned BP, where armchair and zigzag directions are along the *x* axis and *y* axis, respectively. (b) Patterned BP. The symbols α and θ represent the azimuth and elevation angles of incident light, respectively.

conventional FDTD method, whereas the implicit FDTD can break through the CFL factor s_w due to its unconditional stability. However, how to choose maximum CFL factor s will be a vital problem.

In general, FDTD results are affected by spatial sampling and temporal sampling densities. The spatial sampling density refers to the number of points per wavelength (PPW) at the highest frequency in the interested frequency band, while the temporal sampling density represents the number of points per period (PPP) at the highest frequency. The spatial sampling and temporal sampling densities are respectively expressed by

$$Q_{s,w}(\text{PPW}) = \frac{\lambda_{\min}}{\Delta w} = \frac{c_0}{f_{\max}\Delta w} \tag{43}$$

$$Q_t(\text{PPP}) = \frac{T_{\min}}{\Delta t} = \frac{1}{f_{\max}\Delta t} \tag{44}$$

where minimum wavelength λ_{min} and period T_{min} are restricted by the maximum frequency f_{max} of input impulse.

The design of proposed photonic nanostructures based on the monolayer BP with/without patterning is shown in Fig. 1. The structure consists of an alumina (Al_2O_3), a substrate, and a monolayer BP with/without patterning, respectively, shown in Fig. 1(a, b). The whole nanostructure in size is finished with a 67 nm $\times$67 nm$\times$50.25 nm FDTD domain, and its space is discretized with a uniform grid with $\Delta x = \Delta y = \Delta z = 0.67$ nm. The receiver is placed at (40.2, 40.2, 44.89) nm for all cases.

In our design, the dielectric layers of Al_2O_3 (= 33.5 nm of thickness)and substrate (= 6.7 nm thickness)are assumed to be nonmagnetic ($\mu = \mu_0$), and optically lossless with the refractive index of 1.7 and 1.48, respectively. In addition, the monolayer BP (=2.68 nm thickness), shown in Fig. 1(a, b), is depicted by adopting a simple semi-classical Drude model [21], [22], for both *x* and *y* cases, respectively, defined as

$$\sigma_i = j\boldsymbol{D}_i \Big/ \left(\pi\left(\omega + \frac{j\eta}{\hbar}\right)\right) \tag{45}$$

where i denotes the direction concerned, and $\boldsymbol{D}_i$is the Drude weight, written below

$$\boldsymbol{D}_i = \pi e^2 n/m_i \tag{46}$$

where $m_i(i = x, y)$ are the electron effective mass along x and y directions, and denoted by adopting $m_{cx} = \hbar^2/(2\gamma^2/\varsigma + \eta_c)$ and $m_{cy} = \hbar^2/(2\upsilon_c)$. Both $\varepsilon_x(\omega)$ and $\varepsilon_y(\omega)$ are the dielectric constants of the monolayer BP for both x and y directions, respectively, written below

$$\varepsilon_i = \varepsilon_r + \frac{j\sigma_i}{\varepsilon_0\omega a} \tag{47}$$

Via a series of manipulations of σ_i and $\varepsilon_i(i = x, y)$, we obtain

$$\sigma_i = \frac{A_i}{B_i + j\omega} \tag{48}$$

$$\varepsilon_i = \varepsilon_r - \frac{Q_i}{j\omega} + \frac{Q_i}{B_i + j\omega} \tag{49}$$

where $A_i = -\boldsymbol{D}_i/\pi$, $B_i = -\eta/\hbar$, and $Q_i = A_i/(\varepsilon_0 a B_i)$. As depicted in [22], the parameters of BP are determined by fitting the known anisotropic mass for *x*- and *y*-direction. For BP, we have

$$\gamma = \frac{4a}{\pi}\text{eVm}, \varsigma = 2\text{eV}, \eta_c = \frac{\text{h}^2}{0.4m_0}, \upsilon_c = \frac{\text{h}^2}{1.4m_0}$$

In additions, the relaxation rate can be described via choosing the electronic doping $n = 10^{13}\text{cm}^{-2}$ and $\eta = 10$meV. a is the scale length of the BP, and π/a is the width of the Brillouin Zone in [21], [22].

As shown in Fig. 1, the source is excited by a bipolar square wave pulse with the repetition frequency of 2.5 THz. we here set the window time of 0.16 ps in the horizontal axis to observe the stability of electric field component in the *x*- and *y*- direction at the receiver point.

We test first case on the 3D nanostructures with monolayer BP without patterning with the proposed CFS-CNDS-FDTD method with different temporal discretization density and use the results by the conventional explicit FDTD method and the CFS-ADI-FDTD in [46] as the reference.

The Fig. 2 plots simulation results for a receiver for these three different schemes as obtained with different temporal sampling densities in terms of number of PPP. Corresponding to this sampling density, the CFL number is defined as $CFLN = \Delta t/\Delta t_{\max}^{FDTD}$, where $\Delta t_{\max}^{FDTD}$ is the maximum time interval under the stability condition of the regular FDTD algorithm. It should be noted in Fig. 2 that even at such large *CFLN* values simulation results of the proposed CFS-CNDS-FDTD are just as good as those of both the conventional explicit FDTD and the CFS-ADI-FDTD in [46].

Besides, it is clearly reflected in Table 1 that the proposed CFS-CNDS-FDTD can save massive CPU time as compared with that of the conventional FDTD.

Similarly, it can be also observed that the good agreement can be achieved for the 3D nanostructures with monolayer BP with patterning among these FDTD methods, shown in Fig. 3.

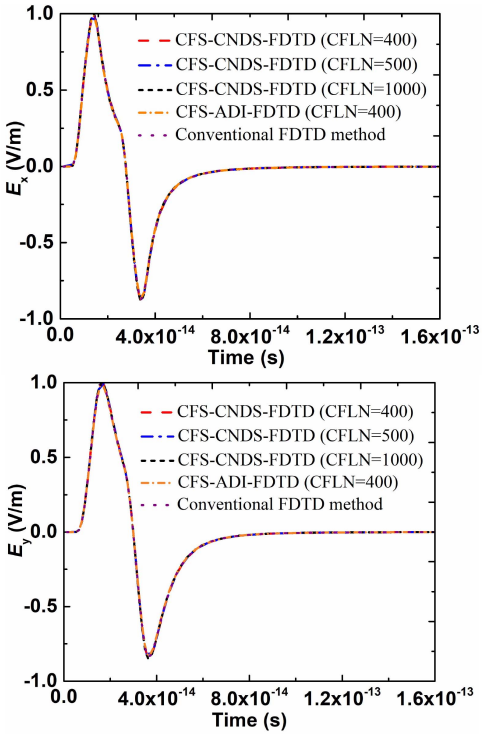

FIGURE 2. Electrical field E_X and E_Y evaluated by the conventional FDTD, the CFS-CNDS-FDTD, and the CFS-ADI-FDTD.

TABLE 1. Computational Time for Different *CFL*Ns

FDTD methods with *CFL*Ns	CPU Time (s)	P (%)
Conventional FDTD method	118000	100
CFS-CNDS-FDTD (CFLN=400)	5462.95	4.6
CFS-CNDS-FDTD (CFLN=500)	4573.83	3.8
CFS-CNDS-FDTD (CFLN=1000)	2232.08	1.8
CFS-ADI-FDTD (CFLN=400)	6612.42	5.6

To show absorption abilities of the proposed CNDS-FDTD, conventional FDTD, and ADI-FDTD based on CFS-PML. We here provide reflective reflection errors of these three methods to compare their absorption accuracies for the case of Fig. 1(a).

It is shown in the above numerical result that the maximum relative reflection errors of Conventional FDTD, CFS-CNDS-FDTD, CFS-ADI-FDTD, are −75.5233 dB, −64.5135 dB, and −54.9536 dB, respectively. As reflected in Fig. 4, therefore, the proposed CNDS-FDTD can obtain better absorption accuracy than the ADI-FDTD.

To further validate the robustness and performance of the CFS-CNDS-FDTD, we next build up and implement the 3D all-dielectric nanostructures with a monolayer BP, which can consist of a BP monolayer (= 2.68 nm of thickness), a Calcium Fluoride (CaF_2) layer (=4.02 nm of thickness), a transparent substrate (=2.01 nm of thickness), the mirror with a stack of dielectric layers of alternate Zirconia (ZrO_2) (=2.01 nm of thickness) and Cryolite (Na_3AlF_6) (=6.03 nm of thickness), and periodic silica (SiO_2) nanoribbons (=3.35 nm of thickness), shown in Fig. 5.

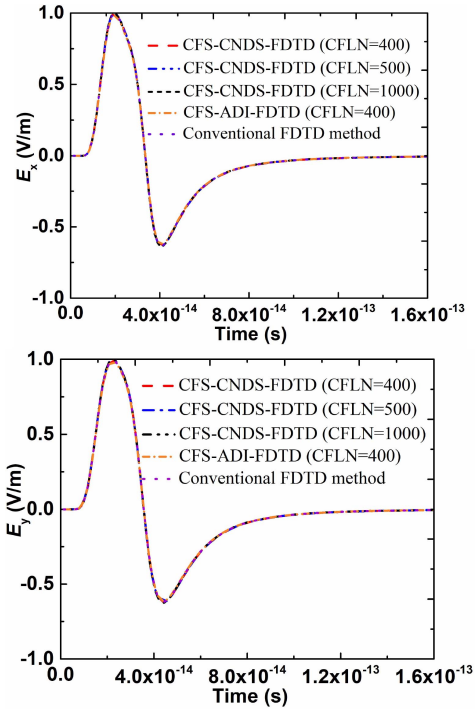

FIGURE 3. Electrical field (a) E_X and (b) E_Y evaluated by the conventional FDTD, the CFS-CNDS-FDTD, and the CFS-ADI-FDTD.

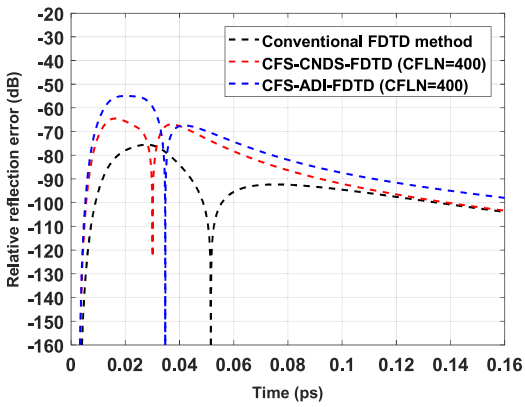

FIGURE 4. Relative reflection error versus time for Conventional FDTD method, CFS-CNDS-FDTD (CFLN = 400), CFS-ADI-FDTD (CFLN = 400).

The whole nanostructure domain is done with a 67 nm × 67 nm × 50.25 nm FDTD domain, and its space is discretized with a uniform grid with $\Delta x = \Delta y = \Delta z =$ 0.67 nm. In our design, the dielectric layers of CaF_2, ZrO_2, SiO_2, Na_3AlF_6 and substrate are assumed to be nonmagnetic, and optically lossless with the refractive index of 1.45, 2.6, 1.48, 1.33, and 1.48, respectively.

In the same way, we here adopt identical source and window time to observe and validate the stability and performance of the CFS-CNDS-FDTD method. The 3D nanostructures adding a monolayer BP without periodic SiO_2 nanoribbons is studied using the proposed CFS-CNDS-FDTD method with different PPP, and then compares the results by the conventional explicit FDTD and CFS-ADI-FDTD methods in [46], shown in Fig. 5(a).

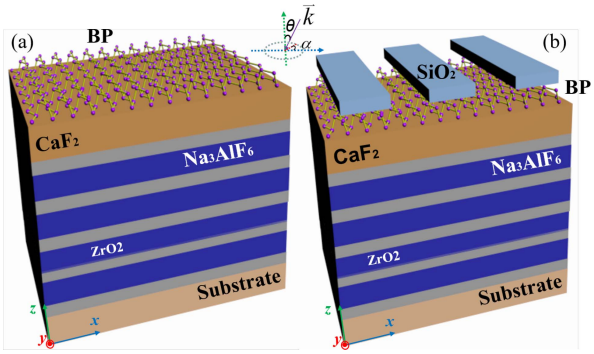

FIGURE 5. (a) Proposed nanostructure adding unpatterned BP without a periodic SiO_2, where armchair and zigzag directions are along the *x* axis and *y* axis, respectively. (b) with a periodic SiO_2. The symbols α and θ represent the azimuth and elevation angles of incident light, respectively.

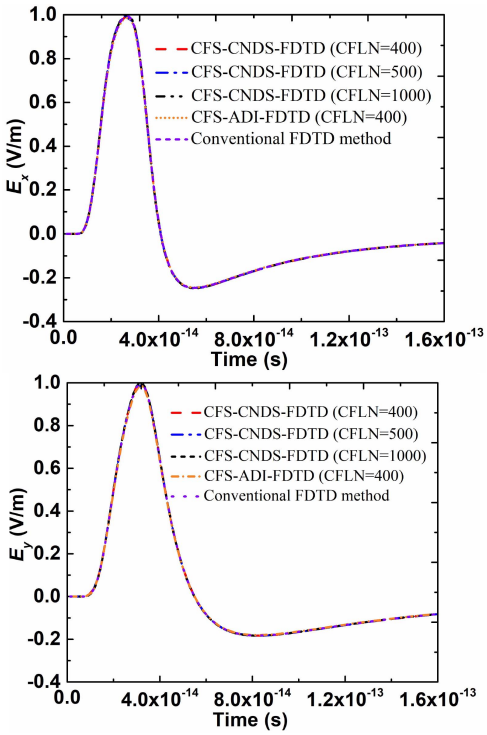

FIGURE 6. Electrical field (a) E_x and (b) E_y evaluated by the conventional FDTD, the CFS-CNDS-FDTD, and the CFS-ADI-FDTD.

TABLE 2. Computational Time for Different *CFL*Ns

FDTD methods with *CFL*Ns	CPU Time (s)	P (%)
Conventional FDTD method	118066	100
CFS-CNDS-FDTD (CFLN=400)	5476.65	4.63
CFS-CNDS-FDTD (CFLN=500)	4598.43	3.89
CFS-CNDS-FDTD (CFLN=1000)	2259.28	1.91
CFS-ADI-FDTD (CFLN=400)	6632.12	5.6

As shown in Fig. 6, the good agreement is obtained among the conventional explicit FDTD, the CFS-ADI- and the CFS- CNDS-FDTDs with different *CFL*Ns. Furthermore, the Table 2 indicates that the proposed CFS-CNDS-FDTD can occupy substantially less CPU time than that of the regular FDTD.

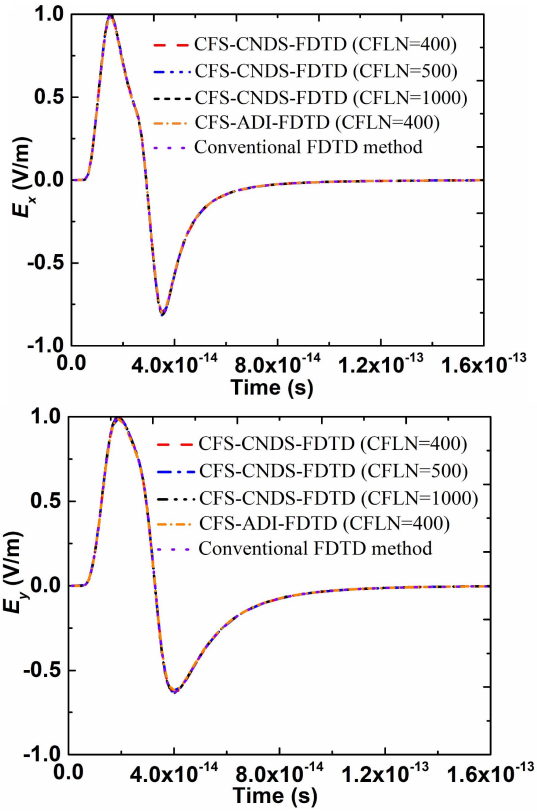

FIGURE 7. Electrical field (a) E_x and (b) E_y evaluated by the conventional FDTD, the CFS-CNDS-FDTD, and the CFS-ADI-FDTD.

Recently, the design of a 3D all-dielectric nanostructure is presented with periodic SiO_2 nanoribbons and 2D graphene in [18], which can obviously enhance light-matter interaction. To further analyze and unveil the physics of periodic structures subsequently, now the periodic SiO_2 is put atop the monolayer BP for validating the accuracy of CFS-CNDS-FDTD method, shown in Fig. 5(b).

As reflected in Fig. 7, we can again observe good agreement among the implicit CN-FDTD and the explicit FDTD methods, therefore, the good performance of the CFS-CNDS-FDTD for modeling all-dielectric nanostructures with BP metasurface is corroborated.

To show absorption abilities of the proposed CNDS-FDTD, conventional FDTD, and ADI-FDTD based on CFS-PML. We here provide reflective reflection errors of these three methods to compare their absorption accuracies for the case of Fig. 5(a).

It is shown in the above numerical result that the maximum relative reflection errors of Conventional FDTD, CFS-CNDS- FDTD, CFS-ADI-FDTD, are -70.0159 dB, -65.0919 dB, and -55.4651 dB, respectively. As reflected in Fig. 8, therefore, the proposed CNDS-FDTD can obtain better absorption accuracy than the ADI-FDTD.

As a result, it will become more practical and efficient if the proposed CFS-CNDS-FDTD method is adopted to solve the 3D all-dielectric nanostructures with the 2DLM

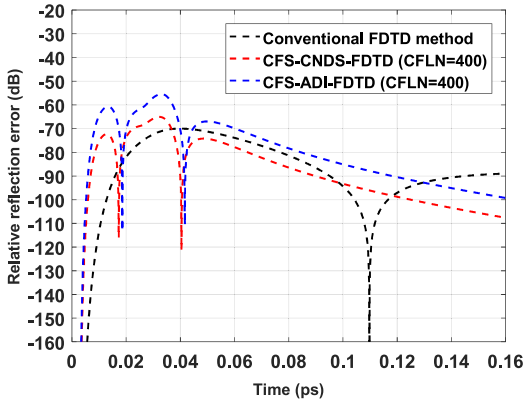

FIGURE 8. Relative reflection error versus time for Conventional FDTD method, CFS-CNDS-FDTD (CFLN = 400), CFS-ADI-FDTD (CFLN = 400).

material in the infrared range instead of the conventional FDTD method.

IV. CONCLUSION

A CFS-CNDS-FDTD has been developed and presented for infrared 2DLM metasurface implementation on all-dielectric nanostructures. The proposed CFS-CNDS-FDTD can greatly improve the computational efficiency when solving infrared terahertz problems with few-atomic-layer thickness of 2DLMs due to possessing capabilities of implicit FDTD method and unsplit-field CFS-PML. As shown in 3D numerical cases, the temporal incremental in CFS-CNDS-FDTD method can reach 1000 times larger than that in the regular FDTD for infrared problems while keeping pinpoint. As a consequence, the CFS-CNDS-FDTD can not only achieve high accuracies and saves several dozen times of CPU time as compared to the regular FDTD, but also pave the road for high-efficient designs of 3D all-dielectric nanostructures with 2DLM metasurfaces.

REFERENCES

[1] A. V. Kildishev, A. Boltasseva, and V. M. Shalaev, "Planar photonics with metasurfaces," *Science*, vol. 339, no. 6125, 2013, Art. no. 1232009.
[2] N. Yu and F. Capasso, "Flat optics with designer metasurfaces," *Nat. Mater.*, vol. 13, no. 2, pp. 139–150, 2014.
[3] P. Genevet, F. Capasso, F. Aieta, M. Khorasaninejad, and R. Devlin, "Recent advances in planar optics: From plasmonic to dielectric metasurfaces," *Optica*, vol. 4, no. 1, pp. 139–152, 2017.
[4] F. Falcone *et al.*, "Babinet principle applied to the design of metasurfaces and metamaterials," *Phys. Rev. Lett.*, vol. 93, no. 19, 2004, Art. no. 197401.
[5] H. H. Hsiao, C. H. Chu, and D. P. Tsai, "Fundamentals and applications of metasurfaces," *Small Methods*, vol. 1, no. 4, 2017, Art. no. 1600064.
[6] M. Khorasaninejad and F. Capasso, "Metalenses: Versatile multifunctional photonic components," *Science*, vol. 358, no. 6367, 2017, Art. no. eaam8100.
[7] M. Khorasaninejad, W. T. Chen, R. C. Devlin, J. Oh, A. Y. Zhu, and F. Capasso, "Metalenses at visible wavelengths: Diffraction-limited focusing and subwavelength resolution imaging," *Science*, vol. 352, no. 6290, pp. 1190–1194, 2016.
[8] N. Yu *et al.*, "Light propagation with phase discontinuities: Generalized laws of reflection and refraction," *Science*, vol. 334, no. 6054, pp. 333–337, 2011.
[9] X. Ni, N. K. Emani, A. V. Kildishev, A. Boltasseva, and V. M. Shalaev, "Broadband light bending with plasmonic nanoantennas," *Science*, vol. 335, no. 6067, p. 427, 2012.
[10] A. Silva, F. Monticone, G. Castaldi, V. Galdi, A. Alú, and N. Engheta, "Performing mathematical operations with metamaterials," *Science*, vol. 343, no. 6167, pp. 160–163, 2014.
[11] F. Monticone, N. M. Estakhri, and A. Alù, "Full control of nanoscale optical transmission with a composite metascreen," *Phys. Rev. Lett.*, vol. 110, no. 20, 2013, Art. no. 203903.
[12] D. Lin, P. Fan, E. Hasman, and M. L. Brongersma, "Dielectric gradient metasurface optical elements," *Science*, vol. 345, no. 6194, pp. 298–302, 2014.
[13] R. Merlin, "Radiationless electromagnetic interference: Evanescent-field lenses and perfect focusing," *Science*, vol. 317, no. 5840, pp. 927–929, 2007.
[14] Z. H. Jiang, D. E. Brocker, P. E. Sieber, and D. H. Werner, "A compact, low-profile metasurface-enabled antenna for wearable medical body-area network devices," *IEEE Trans. Antennas Propag.*, vol. 62, no. 8, pp. 4021–4030, Aug. 2014.
[15] N. Meinzer, W. L. Barnes, and I. R. Hooper, "Plasmonic meta-atoms and metasurfaces," *Nat. Photon.*, vol. 8, no. 12, pp. 889–898, 2014.
[16] C. L. Holloway, E. F. Kuester, J. A. Gordon, J. O'Hara, J. Booth, and D. R. Smith, "An overview of the theory and applications of metasurfaces: The two-dimensional equivalents of metamaterials," *IEEE Antennas Propag. Mag.*, vol. 54, no. 2, pp. 10–35, Apr. 2012.
[17] Y. Yang, W. Wang, P. Moitra, I. I. Kravchenko, D. P. Briggs, and J. Valentine, "Dielectric meta-reflectarray for broadband linear polarization conversion and optical vortex generation," *Nano Lett.*, vol. 14, no. 3, pp. 1394–1399, 2014.
[18] J. Zhou, S. Yan, C. Li, J. Zhu, and Q. H. Liu, "Perfect ultraviolet absorption in graphene using the magnetic resonance of an all-dielectric nanostructure," *Opt. Exp.*, vol. 26, no. 14, pp. 18155–18163, 2018.
[19] M. Faraday, "Experimental relations of gold (and other metals) to light," *Philos. Trans. Roy. Soc. London*, vol. 147, pp. 145–181, Jan. 1857.
[20] L. Zhu *et al.*, "Angle-selective perfect absorption with two-dimensional materials," *Light Sci. Appl.*, vol. 5, Mar. 2016, Art. no. e16052.
[21] T. Low *et al.*, "Plasmons and screening in monolayer and multilayer black phosphorus," *Phys. Rev. Lett.*, vol. 113, Sep. 2014, Art. no. 106802.
[22] Z. Liu and K. Aydin, "Localized surface plasmons in nanostructured monolayer black phosphorus," *Nano Lett.*, vol. 16, no. 6, pp. 3457–3462, 2016.
[23] N. Feng *et al.*, "Near-unity anisotropic infrared absorption in monolayer black phosphorus with/without subwavelength patterning design," *IEEE J. Sel. Topics Quantum Electron.*, vol. 25, no. 3, pp. 1–7, May/Jun. 2019.
[24] J. Wang *et al.*, "The thermal and thermoelectric properties of in-plane C-BN hybrid structures and graphene/h-BN van der Waals heterostructures," *Mater. Today Phys.*, vol. 5, pp. 29–57, Jun. 2018.
[25] J. Wang, W. Lin, X. Xu, F. Ma, and M. Sun, "Plasmon-exciton coupling interaction for surface catalytic reactions," *Chem. Rec.*, vol. 18, no. 5, pp. 481–490, 2018.
[26] N. Feng, Y. Yue, and Q. H. Liu, "Direct *Z*-transform implementation of the CFS-PML based on memory-minimized method," *IEEE Trans. Microw. Theory Techn.*, vol. 63, no. 3, pp. 877–882, Mar. 2015.
[27] N. Feng, Y. Yue, C. Zhu, Q. H. Liu, and L. Wan, "Efficient *Z*-transform implementation of the D-B CFS-PML for truncating multi-term dispersive FDTD domains," *Appl. Comput. Electromagn. Soc. J.*, vol. 29, no. 3, pp. 190–196, 2014.
[28] N. Feng, Y. Yue, C. Zhu, and Q. H. Liu, "Effective implementation of the CFS-PML using DSP techniques for truncating dispersive medium FDTD domains," in *Proc. Progr. Electromagn. Res. Symp.*, 2014, pp. 1127–1130.
[29] N. Feng and J. Li, "Efficient DSP-higher-order PML formulations for the metal plate buried in dispersive soil half-space problem," *IEEE Trans. Electromagn. Compat.*, vol. 54, no. 5, pp. 1178–1181, Oct. 2012.
[30] N. Feng and Q. H. Liu, "Efficient implementation of multi-pole UPML using trapezoidal approximation for general media," *J. Appl. Geophys.*, vol. 111, pp. 59–65, Dec. 2014.
[31] A. Giannopoulos, "Unsplit implementation of higher order PMLs," *IEEE Trans. Antennas Propag.*, vol. 60, no. 3, pp. 1479–1485, Mar. 2012.
[32] N. Feng and J. Li, "Novel and efficient FDTD implementation of higher-order perfectly matched layer based on ADE method," *J. Comput. Phys.*, vol. 232, no. 1, pp. 318–326, 2013.
[33] N. Feng, J. Li, and X. Zhao, "Efficient FDTD implementations of the higher-order PML using DSP techniques for arbitrary media," *IEEE Trans. Antennas Propag.*, vol. 61, no. 5, pp. 2623–2629, May 2013.

[34] N. Feng, Y. Yue, C. Zhu, L. Wan, and Q. H. Liu, "Second-order PML: Optimal choice of *n*th-order PML for truncating FDTD domains," *J. Comput. Phys.*, vol. 285, pp. 71–83, Mar. 2015.
[35] G. Sun and C. W. Trueman, "Unconditionally stable Crank–Nicolson scheme for solving the two-dimensional Maxwell's equations," *Electron. Lett.*, vol. 39, no. 7, pp. 595–597, Apr. 2003.
[36] G. Sun and C. W. Trueman, "The unconditionally-stable cycle-sweep method for 3D FDTD," in *Proc. 10th Int. Antenna Technol. Appl. Electromagn. Symp. URSI Conf.*, Ottawa, ON, Canada, Jul. 2004, pp. 1–4.
[37] G. Sun and C. W. Trueman, "Unconditionally-stable FDTD method based on Crank–Nicolson scheme for solving three-dimensional Maxwell equations," *Electron. Lett.*, vol. 40, no. 10, pp. 589–590, May 2004.
[38] G. Sun and C. W. Trueman, "Approximate Crank–Nicolson schemes for the 2-D finite-difference time-domain method for TE/sub z/wave," *IEEE Trans. Antennas Propag.*, vol. 52, no. 11, pp. 2963–2972, Nov. 2004.
[39] G. Sun, "Development and evaluation of novel finite-difference time domain method," Ph.D. dissertation, Dept. Elect. Comput. Eng., Concordia Univ., Montreal, QC, Canada, 2004.
[40] N. Feng, Y. Zhang, Q. Sun, J. Zhu, W. T. Joines, and Q. H. Liu, "An accurate 3-D CFS-PML based Crank–Nicolson FDTD method and its applications in low-frequency subsurface sensing," *IEEE Trans. Antennas Propag.*, vol. 66, no. 6, pp. 2967–2975, Jun. 2018.
[41] E. L. Tan, "Efficient algorithms for Crank–Nicolson-based finite-difference time-domain methods," *IEEE Trans. Microw. Theory Techn.*, vol. 56, no. 2, pp. 408–413, Feb. 2008.
[42] H. L. Jiang *et al*, "Computationally efficient CN-PML for EM simulations," *IEEE Trans. Microw. Theory Techn.*, vol. 67, no. 12, pp. 4646–4655, Dec. 2019.
[43] P. Y. Wu, H. L. Jiang, Y. J. Xie, and L. Q. Niu, "Three-dimensional higher order PML based on alternating direction implicit algorithm," *IEEE Antennas Wireless Propag. Lett.*, vol. 18, no. 12, pp. 2592–2596, Dec. 2019.
[44] T. Namiki, "3-D ADI-FDTD method-unconditionally stable time-domain algorithm for solving full vector Maxwell's equations," *IEEE Trans. Microw. Theory Techn.*, vol. 48, no. 10, pp. 1743–1748, Oct. 2000.
[45] S. D. Gedney, G. Liu, J. A. Roden, and A. Zhu, "Perfectly matched layer media with CFS for an unconditionally stable ADI-FDTD method," *IEEE Trans. Antennas Propag.*, vol. 49, no. 11, pp. 1554–1559, Nov. 2001.
[46] N. Feng, Y. Zhang, X. Tian, J. Zhu, W. T. Joines, and G. P. Wang, "System-combined ADI-FDTD method and its electromagnetic applications in microwave circuits and antennas," *IEEE Trans. Microw. Theory Techn.*, vol. 67, no. 8, pp. 3260–3270, Aug. 2019.
[47] K. Xu, Z. Fan, D.-Z. Ding, and R.-S. Chen, "GPU accelerated unconditionally stable Crank–Nicolson FDTD method for the analysis of three-dimensional microwave circuits," *Progr. Electromagn. Res.*, vol. 102, pp. 381–395, 2010.
[48] T. Hemmi, F. Costen, S. Garcia, R. Himeno, H. Yokota, and M. Mustafa, "Efficient parallel LOD-FDTD method for Debye-dispersive media," *IEEE Trans. Antennas Propag.*, vol. 62, no. 3, pp. 1330–1338, Mar. 2014.
[49] H. Bao and R. Chen, "An efficient domain decomposition parallel scheme for leapfrog ADI-FDTD method," *IEEE Trans. Antennas Propag.*, vol. 65, no. 3, pp. 1490–1494, Mar. 2017.

NAIXING FENG (Member, IEEE) received the B.S. degree in electronic science and technology and the M.S. degree in micro-electronics and solid-state electronics from Tianjin Polytechnic University, Tianjin, China, in 2010 and 2013, respectively, and the Ph.D. degree from the College of Electronic Science and Technology, Xiamen University, Xiamen, China, in 2018. He studied and worked as a Visiting Scholar supported by the CSC with the Department of Electrical and Computation Engineering, Duke University, USA, from 2015 to 2016. He is currently an Associate Professor with the Institute of Microscale Optoelectronics, Shenzhen University, China. He has published approximately 40 papers in refereed international journals and conferences and is the holder of one patent. His current research interests are mainly in the areas of computational electromagnetics and acoustics, geophysics, nanophotonics, 2-D materials, and their applications.

YUXIAN ZHANG (Member, IEEE) received the B.S. and M.S. degrees from the Tianjin University of Technology and Education, Tianjin, China, and the Ph.D. degree from the College of Electronic Science and Technology, Xiamen University, Xiamen, China, in 2019. He is currently an Associate Professor with the Institute of Microscale Optoelectronics, Shenzhen University, China. His focus is to implement the subsurface electromagnetic imaging in the reverse-time migration method. He has published 21 papers in refereed journals and conference proceedings. His current research interest is computational electromagnetics in the time-domain algorithm. He has received the Chinese National Scholarship three times and participated in the Chinese Graduate Mathematical Contest in Modeling five times with national awards.

QINGSHENG ZENG (Senior Member, IEEE) received the Ph.D. degree from the University of Ottawa, Canada.

He is currently a Distinguished Professor and the Ph.D. Advisor with the Nanjing University of Aeronautics and Astronautics, an Adjunct Professor and the Ph.D. Advisor with the University of Ottawa, Carleton University, Université du Québec an Outaouais, and Institut National de la Recherche Scientifique—Centre Energie, Matériauxet Télécommunications, and a Guest Professor with Harbin Engineering University, Northwestern Polytechnic University, the Beijing University of Post and Telecommunications, and Beijing Jiaotong University. He has been a Research Engineer and a Senior Research Engineer with the Communications Research Centre Canada, Government of Canada. He has published more than 130 SCI and EI indexed papers and technical reports, authored one book, and coauthored two book chapters, one of which has been downloaded more than 3000 times only in one year after it was published in 2011. He has undertaken research and teaching in several fields, including antenna analysis and design, electromagnetic compatibility and interference, ultra wideband technology, radio wave propagation, and computational electromagnetics. He has won several technical and technical service awards, was ranked as one of the researchers at Communications Research Centre Canada with the strongest impacts in 2011, and selected as a distinguished expert under the Plan of Hundreds of Talents of Shanxi Province in China in 2015 and an Oversea Prestigious Advisor of Guangdong Province in 2017. He is the Chair of Antennas and Propagation/Microwave Theory and Techniques Joint Chapter and Secretary of Electromagnetic Compatibility Chapter of IEEE Ottawa, and a member of IEEE Canada Industry Relations Committee. He has been a member of the Strategic Projects Grant Selection Panel (Information and Communications Technologies B) for the Natural Sciences and Engineering Research Council of Canada and the Site Visit Committee of NSERC Industrial Research Chair, and a Reviewer of NSERC Industrial Research and Development Fellowships. His work on the project "Aggregate Interference Analysis and Suitability of Some Propagation Models to Ultrawideband Emissions in Outdoor Environments" has formed one part of the Consultation Paper on the Introduction of Wireless Systems Using Ultra Wideband Technology, Spectrum Management and Telecommunications Policy, Industry Canada, and has been taken as a significant contribution to the International Telecommunication Union. He has been serving as an editorial board member and a reviewer for a number of technical books and scientific journals, as a conference co-chair, a session chair and organizer, a technical program committee co-chair, a member, and a reviewer, and a short course/workshop/tutorial presenter and a keynote speaker for many international and national symposia.

MEI SONG TONG (Senior Member, IEEE) received the Ph.D. degree in electrical engineering from Arizona State University, Tempe, AZ, USA, in 2004.

He was a Research Scientist with the Center for Computational Electromagnetics and Electromagnetics Laboratory, Department of Electrical and Computer Engineering, University of Illinois at Urbana–Champaign, Urbana, IL, USA. He is currently a Distinguished Professor with the Department Head of Electronic Science and Technology and the Vice Dean of the College of Microelectronics, Tongji University, Shanghai, China. He is currently an Adjunct Professor with the University of Illinois at Urbana–Champaign and an Honorary Professor with the University of Hong Kong, Hong Kong. He has published more than 400 papers in refereed journals and conference proceedings, and coauthored six books. His research interests include electromagnetic field theory, antenna theory and design, simulation and design of RF/microwave circuits and devices, interconnect and packaging analysis, inverse electromagnetic scattering for imaging, and computational electromagnetics. He was a recipient of the Visiting Professorship Award from Kyoto University, Japan, in 2012. He advised on and coauthored ten papers that received the Best Student Paper Award International Workshop on Finite Elements for Microwave Engineering in 2014, PIERS2014, PIERS2015, PIERS2016, ICCEM2018, ICCEM2019, PIERS2019, and the International Applied Computational Electromagnetics Society Symposium in 2019, the Travel Fellowship Award of USNC/URSI for the 31st General Assembly and Scientific Symposium of URSI in 2014, the Advance Award of Science and Technology of Shanghai Municipal Government in 2015, the Fellowship Award of JSPS in 2016, the Innovation Award of Universities' Achievements of Ministry of Education of China in 2017, and many teaching related awards from Tongji University and the Shanghai Municipal Government, respectively. In 2018, he was selected as a Distinguished Lecturer by the IEEE Antennas and Propagation Society for the 2019 to 2021 term. He has been the Chair of the Shanghai Chapter and the Chair of the SIGHT Committee of the IEEE Antennas and Propagation Society since 2018. He has served as an Associate Editor or the Guest Editor for several well-known international journals, including *IEEE Antennas and Propagation Magazine*, the IEEE TRANSACTIONS ON ANTENNAS AND PROPAGATION, the IEEE TRANSACTIONS ON COMPONENTS, *Packaging and Manufacturing Technology*, the *International Journal of Numerical Modeling: Electronic Networks*, *Devices and Fields, Progress in Electromagnetics Research*, and the *Journal of Electromagnetic Waves and Applications*. He also served as a Session Organizer, the Session Chair, the Technical Program Committee Member, and the General Chair for some prestigious conferences in the electromagnetics community, such as the IEEE International Symposium on Antennas, the Propagation and USNC/URSI National Radio Science Meeting, the Progress in Electromagnetics Research Symposium, and the IEEE International Conference on Computational Electromagnetics. He is a fellow of Electromagnetics Academy, the Japan Society for the Promotion of Science, a Full Member (Commission B) of the U.S. National Committee for the International Union of Radio Science, and a member of the Applied Computational Electromagnetics Society and the Sigma Xi Honor Society.

WILLIAM T. JOINES (Life Fellow, IEEE) was born in Granite Falls, NC, USA. He received the B.S.E.E. degree (High Hons.) from North Carolina State University in 1959, and the M.S. and Ph.D. degrees in electrical engineering from Duke University in 1961 and 1964, respectively.

He is currently a Professor with the Sensing and Signals Group, Department of Electrical and Computer Engineering, Duke University, where his research and teaching focuses on electromagnetic field and wave interactions with materials and structures, especially in the microwave and optical frequency ranges where wavelengths are commensurate with important structures (antennas, circuit elements, and the human body). From 1959 to 1966, he was a Member of the Technical Staff with Bell Telephone Laboratories, where he was engaged in research and development of microwave components and systems for military applications. He also served as a Radar Technician with U.S. Air Force. He has supervised more than 60 graduate students in their thesis and dissertation research leading to their M.S. and Ph.D. degrees. He has authored or coauthored over 300 technical papers on electromagnetic wave theory and applications, and holds 21 U.S. patents. He was a recent recipient of the Outstanding Engineering Educator Award from the IEEE, and the Scientific and Technical Achievement Award presented by the Environmental Protection Agency in 1982, 1985, and 1990.

GUO PING WANG received the Ph.D. degree from Sichuan University. He was also a Postdoctoral Fellow at Osaka University and a Visiting Scholar at the Tokyo Institute of Technology, Hong Kong University of Science and Technology, and Nanyang Technological University. After that, he was a second rank Professor with Wuhan University and a Distinguished Professor with Luojia Scholar. For his excellent work, he received numerous awards, including the second class of the State Natural Science Award, the first class of the Hubei Natural Science Award, the first class of the Hubei Education Achievements Award, and the first session of the Excellent University Key Teacher Award of the Ministry of Education of China. He is currently a Distinguished Professor with Shenzhen University, honored as being among the National Leading Talents in Shenzhen. Additionally, he was rewarded the National Natural Science Foundation of China for Distinguished Young Scholars, the State Council Special Allowance, and supported by the Program for New Century Excellent Talents in University of Ministry of Education of China. He is a fellow of the Information Science Department and the Mathematical and Physical Science Department of the National Natural Science Foundation of China, and presides over more than 20 projects, including the National Science Foundation of China for Distinguished Young Scientists, the National Basic Research Program of China (973 Program), the Key Program of the National Natural Science Foundation of China, and the Program for New Century Excellent Talents in University of Ministry of Education of China. He obtained several innovative achievements in the research of optical metamaterials, optical super-resolution imaging and sensors, optical cloaking, nanophotonics, and other frontiers, and has published more than 90 peer-reviewed journal papers with more than 50 papers being published on *Nature Communication*, *Physical Review Letters*, *Physical Review B: Rapid Communications*, *Applied Physics Letters*, *Optics Letters*, *Optics Express*, *Nanoscale*, and *Scientific Reports*. In addition, he has contributed to more than 20 invited talks in international conferences and coauthored the book *Plasmonic Nanoguides and Circuits*.